Spin-triplet supercurrents of odd and even parity in nanostructured devices

Lahabi, K.

5

GENERATING SPIN-TRIPLET SUPERCURRENTS WITH A FERROMAGNETIC VORTEX

Generating long-range spin-triplet Cooper pairs requires some form of magnetic inhomogeneity at the interface with a superconductor. This is usually realized using multiple ferromagnets with non-collinear magnetization. Controlling the magnetization of individual ferromagnets however is a highly challenging task. A more efficient method would be to implement the spin texture of a single ferromagnet. We demonstrate this here in a lateral disk-shaped Josephson junction with a cobalt weak link. In this case, the spin-triplet supercurrent is generated by the in-plane exchange field gradient of a magnetic vortex in a cobalt microdisk. Moreover, we show that such devices offer a distinct capacity for controlling the phase, amplitude and spatial distribution of supercurrent in a dynamic fashion. This opens up new possibilities for the realization of superconducting logic and non-volatile memory elements.

As yet unpublished due to a patent application on "spin-textured Josephson junctions".

5.1. MOTIVATION

We begin this chapter with a follow-up experiment on the device introduced in Chapter 4, where we showed how the path of spin-triplet supercurrents can be modified by the magnetic structure of a Co (60 nm)/Ni (1.5 nm) bilayer in a disk-shaped Josephson junction. The purpose of this experiment is to demonstrate a different aspect of our device, one which concerns the *phase* of spin-triplet channels. This subject is revisited in the next section, where we discuss the triplet supercurrents generated by a single ferromagnetic vortex.

5.1.1. FORMATION OF 0-π TRIPLET CHANNELS: S/F'/F/F"/S

Figure 5.1 **a** shows critical current measured while scanning the magnetic field in x-direction $I_c(H_x)$ i.e. field is applied parallel to the trench that defines our weak link (see Figure 4.3 for more details). We begin at $H_x = 0$, where critical current is at its maximum. In this state (labeled **A**), an out-of-plane measurement would produce the double-slit interference pattern, which was described in section 4.2.4. This is also shown in Figure 5.1 **b**, for both negative and positive bias currents. It is important to remember that in state **A**, $I_c(H_z)$ has a single maximum close to zero field. This is independent of sweep sequence or direction of H_z[1].

As we increase H_x, the magnetic vortex in Co begins to move in y-direction, away from the trench (vortex moves perpendicular to the applied field). This results in a rapid suppression of supercurrent, which completely disappears for $H_x \gtrapprox 20$ mT. Remarkably, $I_c(H_x)$ remains heavily suppressed even when the field is brought back to zero (**B**). Although there is a noticeable rise at $H_x \approx -20$ mT (**C**), the junction only retains its maximum critical current at -45 mT (**D**). At first glance, it may seem that the observed suppression of I_c is simply due to the lack of magnetic non-collinearity (MNC), necessary for generating long-range triplet current. This however would be far from accurate, as our simulations and out-of-plane interferometry measurements reveal.

Micromagnetic simulations with an in-plane field indicate that, during the magnetization reversal, the vortex is not simply brought back, but that an intermediate configuration exists with up to three vortices which converge into a single vortex state at sufficiently large negative magnetic fields. This corresponds to transition at **D** in Figure 5.1, where the critical current recovers its maximum value. Figure 5.1 **c** shows an $I_c(H_z)$ pattern, taken while the system was in the 'suppressed current' state. The experimental setup used for these measurements could only provide magnetic fields in one direction. Hence, to obtain the results shown in Figure 5.1 **c**, we stopped the in-

[1] In some field sweeps the $I_c(H_z)$ maximum may appear slightly shifted (by less than 2 mT), there are however no discernable changes in the pattern itself.

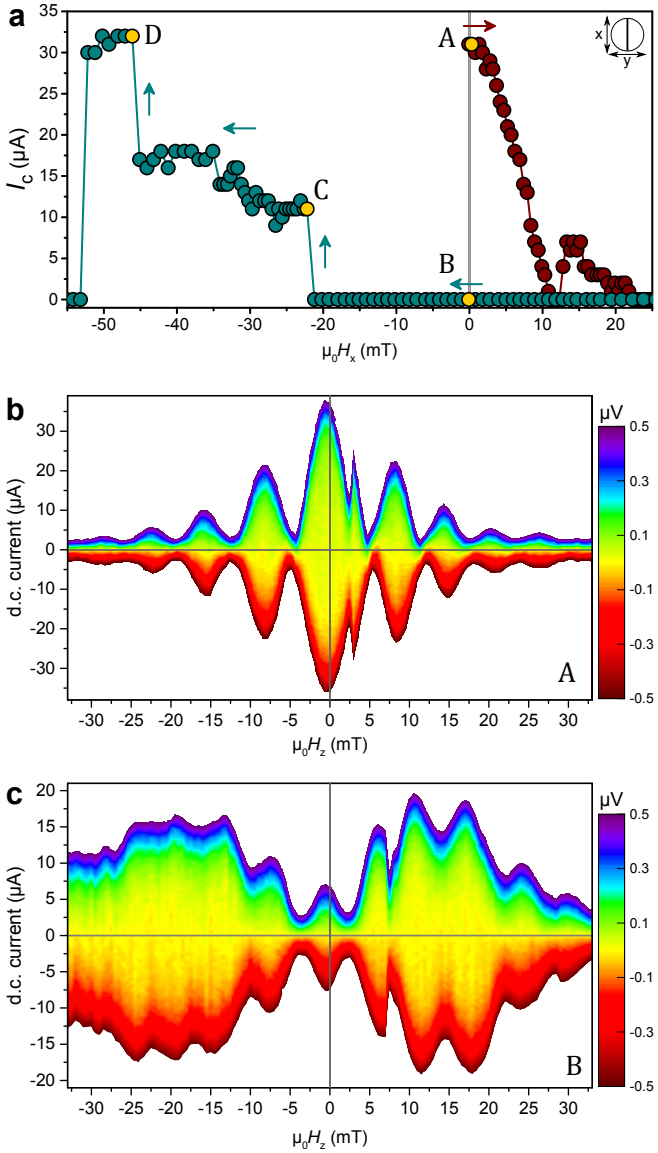

Figure 5.1: **stable states of the Co-Ni disk: interference patterns from different transport states. a**, I_c measured as a function of H_x for forward (wine) and reverse (cyan) field sweep directions, at 2.1 K. Inset shows the x and y directions with respect to the orientation of the junction barrier. The H_x sweep sequence was $0 \rightarrow +150$ mT $\rightarrow -150$ mT. The field sweep was stopped at **A** and {B to measure the interference patterns shown in **b** and **c**, respectively. **b,c** were obtained by sweeping the out-of-plane field H_z as +35 mT $\rightarrow -35$ mT, while the in-plane field is zero. Reducing the field range did not affect the I_c behaviour shown here. **b** is the double-slit interference pattern with maximum I_c at zero field, described in Chapter 4. **c** I_c is suppressed at zero field, and has high-field maxima in *both* directions.

plane field sweep at $H_x \approx 0$, turned the sample plane by 90° (so that $H \parallel z$), and then continued by measuring $I_c(H_z)$. While $I_c(0)$ is initially suppressed, it grows larger as we sweep the field in either direction. In contrast to the initial pattern **A**, the main maxima occur at $\approx \pm 12$ mT or higher. Had there been no triplet generation in our device (e.g. due to lack of MNC), I_c would have remained constantly suppressed throughout the H_z sweep. The reason for measuring a reduced I_c at small fields is not absence of triplet supercurrents, but rather their *presence* in the form of spontaneous supercurrents.

Suppression of $I_c(0)$ and high-field maxima[2] in the interference pattern are the universal characteristics of Josephson junctions with multiple 0 and π segments arranged in parallel (the so-called 0-π junction). Such systems have been realized in zigzag-shaped d-wave/s-wave [1] and S/F/S junctions, where step-like changes in the thickness of the F layer can be used to create an array of 0 and π segments [2, 3] (short-range proximity effect). This means that the critical current density J_c needs to alternate its sign along the junction as $J_c^0 \approx -J_c^\pi$. As the phase varies from 0 to π (and vice versa), it creates a spontaneous circulating current around the 0-π boundary. The spontaneous supercurrent also carries a vortex with the total flux of $\pm\Phi_0$. If the 0 and π segments are equal in size and critical current density $J_c^0 = -J_c^\pi$, the junction has no capacity for an additional bias current, which appears as $I_c = 0$ in a transport measurement. Applying an external field compensates for the built-in phase variations in the junction, and allows for constructive interference of currents between the 0 and π segments, which in turn leads to the enhancement of I_c.

The interference pattern of a given 0-π junction depends on the exact number, size and arrangement of the 0 and π channels, as well as their critical current densities. In our device these parameters are determined by the number and configuration of the magnetic vortices in Co, as well as the relative alignment of the Ni layer in the left and right side of the junction. The former defines the size and the number of channels (since each vortex interrupts the flow of supercurrent), and the latter determines their phase (see 3.5). If the magnetic orientation of the left Ni layer is *locally* parallel (antiparallel) to that on the right side, the channel behaves as a π (0) junction. This concept is illustrated in Figure 4.S1. Unlike the Co disk, the 1.5 nm thick Ni layer does not have a robust magnetization pattern. As shown in Figure 4.S2, its magnetic texture is not fully decoupled from the transport leads connected to the disk, and can be easily disturbed by the magnetization of Co. While every simulation shows the magnetic moments of Ni to lie along the trench ($\parallel x$), the relative orientation of the left and right sides can change. Estimating the Ni magnetization becomes even more challenging if there are multiple vortices in the Co, due to the strong coupling to the local dipole fields from each vortex core.

[2] Interference pattern for a single field sweep needs to have maxima in both positive and negative fields. This is to exclude self-fields of the ferromagnets, which can only introduce a field offset in the original interference pattern.

To summarise, the main obstacle here is that there are no reliable means to control the magnetic structure of the Ni (1.5 nm) layer on both sides of the junction. While this does not prevent us from generating long-range triplet currents, and regulating their spatial distribution, it does limit our capacity to control the phase. We resolve this in the next section by removing the Ni layer, and utilizing the vortex magnetization of the Co disk to generate and control long-range triplet supercurrents.

What makes the results of Figure 5.1 already promising is that there are two stable zero-field states, corresponding to maximum and minimum I_c (**A** and **B**, respectively). For each state, the device was warmed up to room temperature, stored in a vacuum chamber for a finite number of days (often weeks) and measured again. We found no discernable changes in the value of I_c or the interference pattern before the warm-up. This represents a promising new outlook for the realization of non-volatile superconducting memory elements.

5.2. GENERATING SPIN-TRIPLET SUPERCURRENTS WITH A FERROMAGNETIC VORTEX

Triplet supercurrents are commonly generated by a ferromagnetic trilayer S/F'/F/F"/S, where F' and F" can have non-collinear magnetizations. In terms of control over supercurrents, the full potential of such systems is only realised if the magnetization of each ferromagnet can be regulated independently. There are however alternatives to this. It has been proposed that the spin structure of a ferromagnetic vortex can be used to generate long-range triplet correlations [4, 5]. Here we demonstrate this in disk-shaped Josephson junctions, where the superconducting electrodes are separated by a cobalt barrier (≈ 20 nm long). Figure 5.2 shows the schematic of our device. The system contains two key elements. One is the *in-plane* gradient of the exchange field, responsible for generating the long-range triplet correlations, and the other is the vortex core, where the local magnetization turns out-of-plane. The core plays a key role by suppressing the long-range triplet component [4]. Sample preparation followed the same procedure as the one described in Chapter 4. The only difference here is the absence of the Ni (1.5 nm) layer.

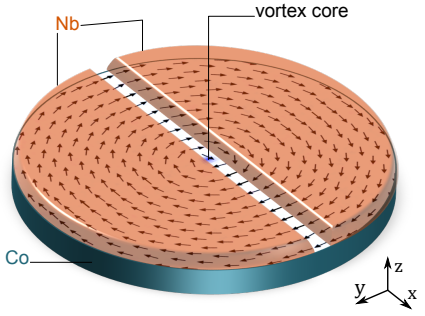

Figure 5.2: Schematic of the device. Superconducting electrodes are deposited directly on the Co, with no additional magnetic layers. The junction is formed by opening a gap (≈ 20 nm) in the Nb layer, leaving only Co in the weak link. The arrows represent the simulated magnetic pattern in Co. At the vortex core the magnetic moments turn sharply out-of-plane (blue pixels).

5.2.1. BASIC TRANSPORT AND GROUND STATE INTERFERENCE

Figure 5.3 shows the typical transport behavior of a Co disk junction with long-range triplet currents. In the absence of in-plane fields, the ground state of our system corresponds to a single vortex at the centre of the disk. While in this state, transport characteristics are similar to those of the Co-Ni disk from Chapter 4. This is shown in Figure 5.3, where we see a double-slit interference pattern (i.e. lobes with a similar width). The two systems however reveal their differences in in-plane measurements.

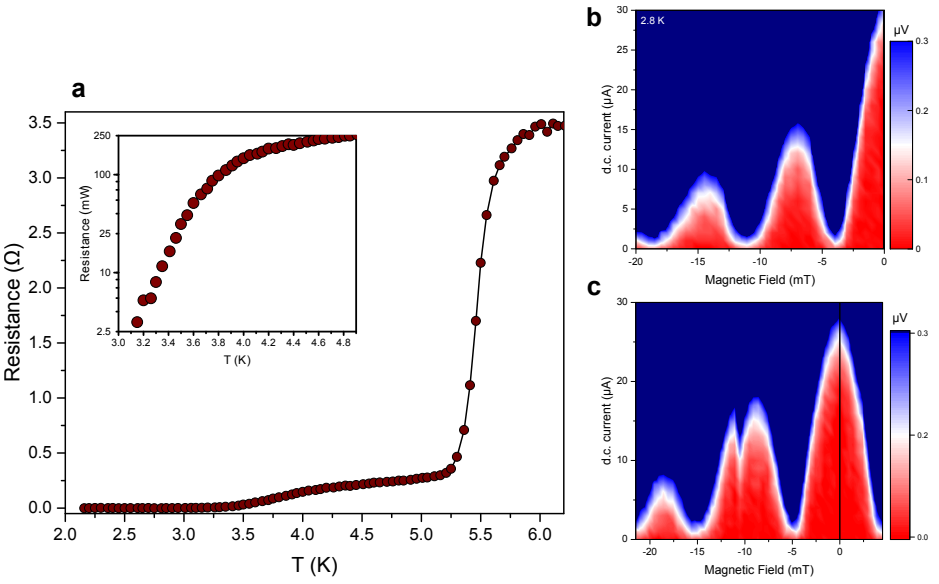

Figure 5.3: **Co disk: transport at ground state magnetizationa**, resistance as a function of temperature $R(T)$, measured using a 10 μA current bias. $R(T)$ shows two distinct transitions, with the one at lower temperatures corresponding to the junction, andis shown on a logarithmic scale in the inset. **b,c** interference patterns at 2.8 K, measured while sweeping the out-of-plane field from 0 to +20 mT (**b**), and from 21 mT to −5 mT (**c**). Both sweeps correspond to a double-slit interference pattern, and I_c has a single maximum at zero field, regardless of sweep direction.

5.2.2. MAGNETOTRANSPORT WITH IN-PLANE FIELDS

In-plane fields can alter the magnetic structure of our junction by displacing the vortex core in a perpendicular direction. Figure 5.4 **a** shows the critical current of Co disk junction; measured as a function of $H_y \perp$ trench. This corresponds to a vortex displacement along the trench. In order to show the contrast, Figure 5.4 **b** presents the same measurements carried out on the Co-Ni disk (taken from the previous chapter). Initially, at $H_y = 0$, both systems show maximum critical current. As we sweep the field to 15 mT, the critical current of the Co disk drops to zero. This field regime corresponds to maximum vortex core displacement ≈ 20 nm per mT (estimated from micromagnetic simulations). We also observe an abrupt suppression of supercurrent in Co-Ni device at $H_y = 7$ mT. This however occurs over a narrow field range ≈ 2 mT, and I_c is recovered by $H_y = 10$ mT. In contrast, supercurrent transport in the Co disk remains suppressed up to 25 mT. Yet, our simulations show the vortex to be present in the disk up to $H_y = 40 \pm 5$ mT. We attribute the suppressed I_c in this field range to the phase difference between the triplet channels, which develops when we disrupt the axisymmetric pattern of the ferromagnetic vortex. This causes the system to act as a 0-π SQUID, and is discussed later in this section.

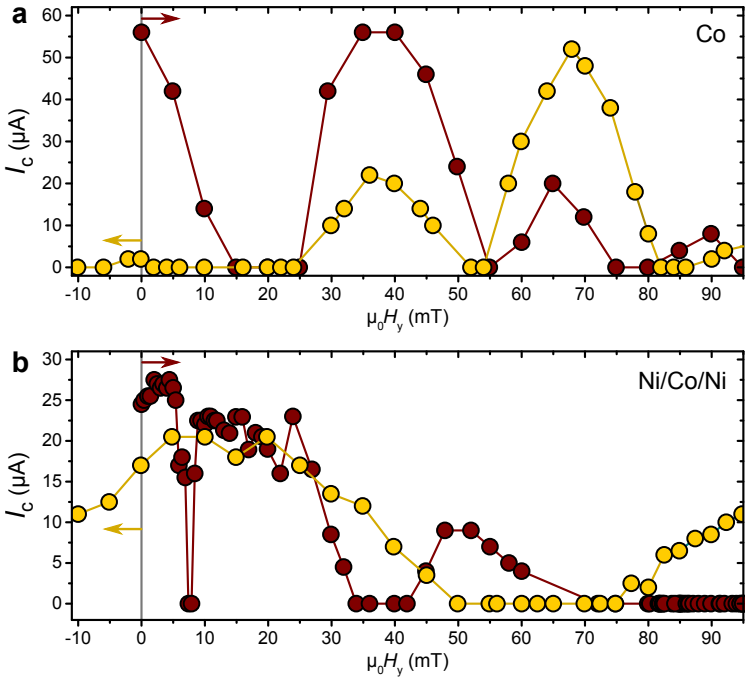

Figure 5.4: **In-plane measurements: Co disk vs. Co-Ni disk.**, I_c measured as a function of H_y, for forward (wine) and reverse (yellow) field sweeps. The sweep sequence followed as $0 \rightarrow +150$ mT $\rightarrow -150$ mT. **a**, shows the behaviour of the Co disk, which is the focus of this chapter. **b**, corresponds to the same sequence of measurements from the Co-Ni disk, and is presented here to highlight the contrast between the two systems. The most notable one being the behaviour of I_c during the field reversal, where the Co disk maintains $I_c \approx 0$ at zero field.

I_c grows rapidly as we increase the field above 25 mT, and even recovers the original (zero field) maximum, before it sharply declines at 45 mT. In our simulations this corresponds to the vortex core being pressed against the edge of the disk (on one side of the junction), and subsequently exiting the system at $H_y \gtrsim 45$ mT. Note that the reentrant superconductivity observed in the Co disk is substantially larger than that of the Co-Ni device, and occurs over a different field range (e.g. at 40 mT I_c is maximum in the Co disk, but is zero for the Co-Ni device). We also observe small but finite peaks up to 90 mT. Although we cannot identify their origin at this stage, these might correspond to some form of local spin texture in Co (e.g. buckling).

We continue to magnetize the system by sweeping up to 150 mT, at which point we reverse the sweep direction. As we reduce the field back to zero (yellow), we find a highly unusual behavior, where I_c is maximum at 68 mT but is heavily suppressed around zero field. This $I_c(H_y)$ pattern is also robust with respect to sweep direction. Following the same measurement protocol with negative field would mirror the pattern point by point, i.e. $I_c(-H_y)_{\text{(reverse)}} = I_c(+H_y)_{\text{(forward)}}$. Hence, sweeping in both

directions results in a suppressed I_c at zero field. This however could be fully reversed by reconditioning the system with fields of 50 mT or higher, which brings back the original SQUID pattern with maximum I_c appearing at zero field.

Micromagnetic simulations indicate that during such field reversal, our system goes through a range of nonuniform magnetic patterns, which can have profound consequence for the phase and distribution of long-range triplet supercurrents. These include various forms of buckling (e.g. the so called S and C states), as well as multiple vortices and saddle points which appear at $H_y = 0$. A discussion on these states is however beyond the scope of this chapter. Instead, here we focus on the single vortex state, which is arguably the most robust and controllable magnetic pattern.

5.2.3. EMERGENCE OF 0 & π CHANNELS IN THE VORTEX

It was proposed by Kalenkov *et al.* [5], that both zero and π junctions can be realized with the long-range triplet components in a ferromagnetic vortex. More specifically, they predict the junction to be in the π state when the superconducting electrodes are not symmetric with respect to the vortex magnetization pattern. They proposed to realize this by asymmetric geometries for the superconducting electrodes placed on the vortex. However, the same situation can in principle be created by breaking the axisymmetric pattern of the vortex, as we do here by applying an in-plane field, which produces an asymmetric magnetic pattern with respect to the electrodes. There is however one crucial difference between our system and the ones described in Ref. [5], and it concerns the vortex core. The above-mentioned theoretical framework was formulated for a system with a fully in-plane magnetization, as the core ($\lesssim$ 20 nm) is deemed to be too small (compared to the coherence length) to play a significant role. This is a sound and practical assumption. As we have seen however, the local magnetization of the vortex core tends to be highly effective in suppressing long-range triplet currents. This leads to the formation of two transport channels, either one of which can be in the zero or π regime. Hence, the system has the capacity to act as a SQUID with four possible configurations: 0-0, π-π, 0-π and π-0. The controllable nature of a magnetic vortex allows for the implemention of in-plane fields to switch between these modes by changing the magnetization pattern in a reversible manner. We explore this in the following section with the use of a vector magnet.

5.2.4. INTERFERENCE PATTERNS FROM A DISPLACED VORTEX

The core of the ferromagnetic vortex can be freely displaced by applying relatively small magnetic in-plane fields ($\lesssim$ 40 mT). Once the field is removed however, magnetization will return to its original state, with the core positioned at the centre of the disk. While in this state, superconducting quantum interferometry (SQI) measure-

ments yield a double-slit pattern, with $I_c(H_z)$ being maximum at zero field, which could correspond to either a 0-0 or a π-π SQUID configuration. The exception to this is when we drive the vortex out of the disk by applying a sufficiently large in-plane field. In this case, removing the field would transform the magnetization to a metastable state with multiple vortices present in the disk[3]. SQI patterns from this state are similar to those of junctions with multiple 0-π segments (...0-π-0-π-0...), which are characterized by a suppressed $I_c(H \approx 0)$ and high-field maxima (e.g. see Figure 5.1 **c**). However, the complex magnetic pattern of the metastable state, combined with unusual interference patterns, prevent us from developing a comprehensive description of the phase and number of transport channels involved. A systematic approach would be to reduce the problem to a single vortex; and examine the $I_c(H_z)$ patterns, measured while the core is displaced by a constant H_{xy} field.

The measurements presented so far were carried out in a Physical Properties Measurement System (PPMS) by Quantum Design, where magnetic field can be applied in only one direction. While we could switch between in- and out-of-plane configurations by (mechanically) turning our sample, the setup cannot support $I_c(H_z)$ measurement in presence of a finite H_{xy}. Hence, SQI measurements could only be applied to the states that are stable at zero in-plane field. We overcome this limitation with the use of a cryostat equipped with a "vector magnet", which allows us to control the applied field in x, y and z directions separately.

Figure 5.5 shows the $I_c(H_z)$ patterns, taken while applying constant H_x fields. For each value of H_x, we also present the simulated magnetic pattern (right panel), with the line representing the gap in Nb. It should also be mentioned that this is a different sample than the one presented in the previous section (its basic transport properties are however very similar). In the absence of in-plane fields, the vortex core is situated at the centre of the disk, and we observe our usual double slit interference pattern, with maximum I_c at zero field (Figure 5.5 **a**).

We then proceed by sweeping H_x to 10 mT, where we find an abrupt suppression of I_c. In this state, the interference pattern is still very much SQUID-like, as the lobes appear to be similar in width. Instead of a maximum however, $I_c(H_z)$ now has a minimum at zero field. For a SQUID device, this pattern would correspond to a 0-π state. Our simulation for this field shows the core to be displaced along y. As the magnetic pattern is no longer symmetric with respect to the superconducting electrodes, the formation of a π channel would also be consistent with the predictions of Ref. [5].

Before we continue with the results, it is important to note that the observed suppression of $I_c(H_z \approx 0)$, which we attribute to a 0-π SQUID state, cannot be produced by self-fields (i.e. stray fields) from the ferromagnet, or a field offset in our measure-

[3] these states are stabilised by the Co in the transport leads, connected to the sides of the disk, which modify the shape anisotropy. Such states are usually absent in symmetric magnetic dots.

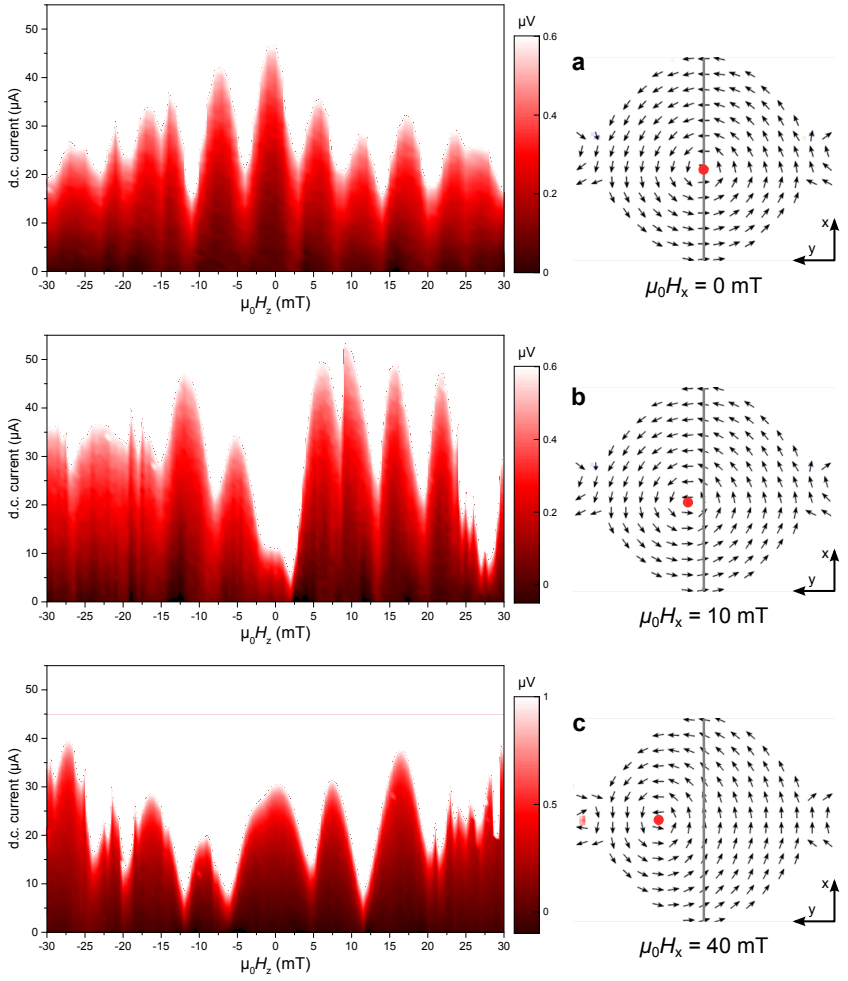

Figure 5.5: **Supercurrent interference with different magnetic patterns.** The left panel shows the interference patterns, measured by scanning H_z from +30 mT to −30 mT, in steps of 0.5 mT, while fixing H_x at 0 mT (**a**), 10 mT (**b**) and 40 mT(**c**) during a forward H_x sweep. The right panel shows the simulated magnetic patterns for the specified H_x fields. The grey line in the middle disk represents the junction barrier, and the red dot indicates the position of the vortex. At $H_x = 0$ (**a**) the core is located in the middle of the junction, which yields a double-slit interference pattern, with all lobes having the same width, and a maximum I_c at zero field. **b**, $H_x = 10$ mT breaks the symmetry of the system by slightly shifting the core from the centre. The interference pattern is similar to that of a 0-π SQUID: I_c is suppressed for $H_z \approx 0$, the lobes maintain a similar size and the pattern appears to be shifted with respect to $H_z = 0$. **c**, the core is displaced by over 100 nm from the centre. I_c shows an entirely different behaviour, and cannot be described by a two-channel transport.

ment setup. Firstly, the same $I_c(H_z)$ patterns could be reproduced, regardless of how we sweep H_z. For each H_x shown in Figure 5.5, we measured the interference pattern while sweeping H_z as $0 \rightarrow +30$ mT, $+30$ mT$\rightarrow -30$ mT and -30 mT$\rightarrow +30$ mT, in steps of 0.5 mT. The same SQI behaviour was found in all three patterns. Secondly, here we are only comparing the interference patterns with *each other*. Even if there is a finite error in the absolute value of the applied field, this would not change the interference patterns relative to each other. Lastly, and most importantly, for every triplet device we measure, there is also a control device (located on the same substrate), where the junction transport is carried out by singlet currents (for details on control experiments, see Section 4.4.4 and Figure 4.S5). Despite having the same Co structure, the singlet junctions exhibit none of the effects described above. These devices consistently yield a Fraunhofer pattern (single-slit), and exhibit no appreciable dependence on in-plane fields. While reconditioning the magnetization could in some cases shift the $I_c(H_z)$ maximum by up to ≈ 2.5 mT in *one* direction (most likely by switching the vortex polarity), the Fraunhofer pattern itself remains unchanged.

Figure 5.5 **c** shows the SQI pattern taken at $H_x = 40$ mT, where we find $I_c(0)$ to recover. At this point in the simulation, the core is over 100 nm away from the junction barrier (i.e. the trench). We find an unusual interference pattern, which itself appears to be a combination of different patterns. The central lobe is similar to that of Fraunhofer (i.e. twice as wide as the subsequent ones). Instead of decaying however, the supercurrent grows larger with the field. We are not aware of any system where a similar interference pattern has been observed, and hence can only speculate about its origin. Nonetheless, a crude inverse Fourier analysis of the pattern suggests the presence of three separate transport channels, with the smallest one located in the middle of the weak link.

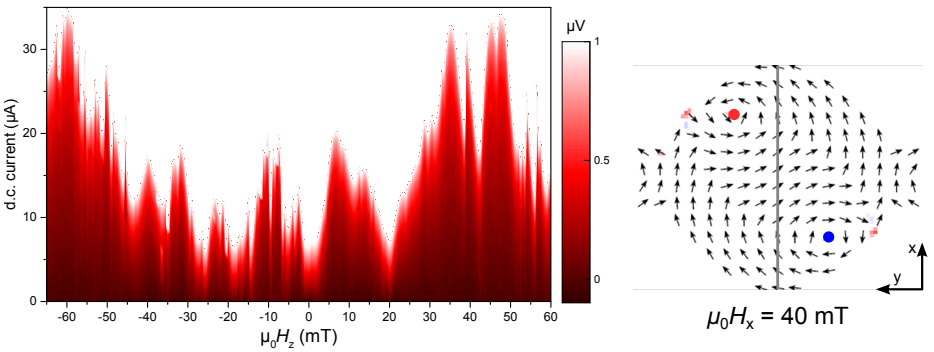

Figure 5.6: I_c behaviour at $H_x = 40$ mT, measured during the reverse H_x sweep. Micromagnetic simulations show that while reversing H_x from 150 mT, two vortices entre the disk at $mu_0 H_x \approx 40$ mT, as shown in right panel. Red and blue represent positive and negative polarities, respectively. In contract to the interference pattern measured during the forward H_x sweep (Figure 5.5 **c**), I_c is heavily suppressed within ± 5 mT, but recovers as we increase the field beyond 30 mT in either directions.

We continue by magnetizing the system with $H_x \rightarrow 150$ mT, and then return the field back to $H_x = 40$ mT to measure a second $I_c(H_z)$ pattern (shown in 5.6). Our simulations show that following this particular field sweep sequence, the disk would be hosting two vortices instead of one, which should profoundly alter the nature of transport in our device. This is indeed the case, as we find an entirely different SQI pattern than the one in Figure 5.5 **c**. While initially I_c is heavily suppressed, it grows larger with the applied field up to 50 mT. We also observe a series of small features which may appear as stochastic discontinuities in some underlying interference pattern. Surprisingly however, we find these features to not be random, as almost every single peak was reproduced in forward and reverse field scans.

5.2.5. SUMMARY & OUTLOOK

Long-range spin-triplet correlations in ferromagnets form a novel platform to control various aspects of supercurrents including their amplitude, phase and spatial distribution. This however, relies on the ability to control the magnetic structure of a device, which so far has typically consisted of a ferromagnetic trilayer S/F'/F/F"/S, where F' and F" need to have non-collinear magnetizations with respect to F. Here we present an alternative to this, where the long-range triplet component is generated by the magnetic pattern of a ferromagnetic vortex. By reducing the number of required ferromagnets to one, this system sets a milestone for the utilization of spin-triplet supercurrents in functional devices.

In contrast to the trilayer system, here the long-range triplet component is induced by the in-plane gradient of the exchange field. We find these correlations to be suppressed by the out-of-plane magnetization of the vortex core, resulting in a two-channel interference pattern[4]. Depending on the position of the vortex core, the two channels can develop a phase difference. For small displacements of the core, we find interference patterns similar to that of a 0-π SQUID. More generally, depending on the position of the vortex with respect to the electrodes, we can yield widely different transport behaviours in the same device (e.g. see Figure 5.5).

In addition to the single vortex state, there are states with multiple vortices (up to three) which can be stabilized by proper conditioning of magnetization. Interference pattern from these states indicate the presence of multiple 0-π regions in our junction. A consequence of this is that there can be two (and possibly more) stable zero-field states with minimum and maximum $I_c(0)$ values (see Figure 5.4 **a**). As these states are defined entirely by the magnetic pattern of a strong ferromagnet (Co), they are highly stable. Even when warmed up and stored at room temperature for long periods (often weeks), upon cooling, we measure the same value of $I_c(0)$.

[4] there is however a distinct possibility for spontaneous currents to emerge *near* the vortex core, due to the non-coplanar magnetic texture. See Ref. [6] for more details.

This introduces a new direction for the realisation of non-volatile superconducting memory, where the bits are stored in the magnetic pattern of a *single* ferromagnet, and are read by measuring the I_c (or rather $I_c R_N$). Even more promising are the possibilities for "writing" the bits. So far we have used static magnetic fields to switch from one I_c state to another. However, magnetic vortices can be displaced and manipulated by pulses in the GHz regime, making this an ideal platform to implement magnetization dynamics for high-speed superconducting electronics.

REFERENCES

[1] H. Smilde, D. Blank, G. Gerritsma, H. Hilgenkamp, H. Rogalla, et al. d-wave–induced Josephson current counterflow in $YBa_2Cu_3O_7$/Nb zigzag junctions. *Physical Review Letters*, 88(5):057004, 2002.

[2] S. Scharinger, C. Gürlich, R. Mints, M. Weides, H. Kohlstedt, E. Goldobin, D. Koelle, and R. Kleiner. Interference patterns of multifacet 20×(0- π) Josephson junctions with ferromagnetic barrier. *Physical Review B*, 81(17):174535, 2010.

[3] C. Gürlich, S. Scharinger, M. Weides, H. Kohlstedt, R. Mints, E. Goldobin, D. Koelle, and R. Kleiner. Visualizing supercurrents in ferromagnetic Josephson junctions with various arrangements of 0 and π segments. *Physical Review B*, 81(9):094502, 2010.

[4] M. Silaev. Possibility of a long-range proximity effect in a ferromagnetic nanoparticle. *Physical Review B*, 79(18):184505, 2009.

[5] M. S. Kalenkov, A. D. Zaikin, and V. T. Petrashov. Triplet superconductivity in a ferromagnetic vortex. *Physical Review Letters*, 107(8):087003, 2011.

[6] M. Silaev. Double-slit Fraunhofer pattern as the signature of the Josephson effect between berezinskiĭ superconductors through the ferromagnetic vortex. *arXiv:1708.07467*, 2017.